Direct Gear Design for Asymmetric Tooth Gears

A. Kapelevich

Abstract In many gear drives, the tooth load on one flank is significantly higher and is applied for longer periods of time than for the opposite one. An asymmetric tooth shape reflects this functional difference. Design intent of asymmetric gear teeth is to improve performance of the primary drive profiles at the expense of the performance off the opposite coast profiles. The coast profiles are unloaded or lightly loaded during a relatively short work period. Asymmetric tooth profiles also make it possible simultaneously to increase the contact ratio and operating pressure angle beyond the conventional gear limits. The main advantage of asymmetric gears is contact stress reduction on the drive flanks, resulting in higher torque density (load capacity per gear size). The paper presents an application of the Direct Gear Design® method to asymmetric tooth gears. This is an alternative approach to traditional design of involute gears, separating gear geometry definition from the generating (tooling) rack to maximize gear drive performance. The paper describes asymmetric tooth and gear mesh characteristics, limits of asymmetric tooth gearing, tooth geometry optimization, analytical and experimental comparison of symmetric and asymmetric tooth gears, and implementation of gears with asymmetric teeth.

Keywords Direct gear design · Asymmetric tooth gears · Gear geometry optimization · Performance maximization

1 Introduction

The flanks of a gear tooth are functionally different for many gear drives. Tooth load on one flank is significantly higher and is applied for longer periods of time than that on the opposite one. An asymmetric tooth shape reflects this functional difference (Fig. 1). A design objective of asymmetric gear teeth is to improve the

A. Kapelevich (✉)
AKGears, LLC, Shoreview, USA
e-mail: ak@akgears.com

V. Goldfarb and N. Barmina (eds.), *Theory and Practice of Gearing and Transmissions*, Mechanisms and Machine Science 34,
DOI 10.1007/978-3-319-19740-1_7

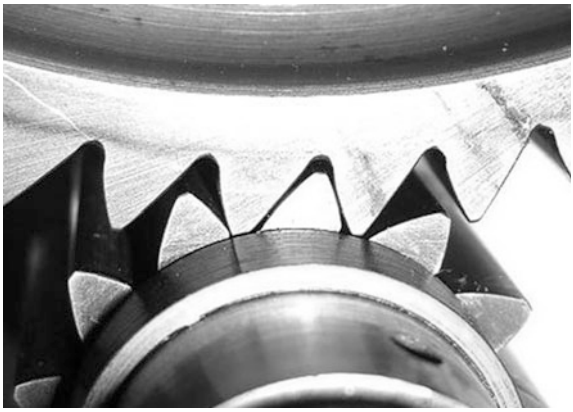

Fig. 1 Gears with asymmetric teeth

performance of primary drive profiles at the expense of the performance of opposite coast profiles. The coast flanks are unloaded or lightly loaded during a relatively short work period.

The first asymmetric gears had a buttress tooth shape with a low pressure angle at the drive tooth flanks, while supporting coast flanks had a high pressure angle. According Woodbury [1]: "In Leonardo da Vinci we find some drawings of tooth form—one very like a buttress tooth." In 1841, Willis [2] had shown the asymmetric buttress gear teeth with the following explanation: "If a machine be of such a nature that the wheels are only required to turn in one direction, the strength of the teeth may be doubled by an alteration of form". Leutwiler [3] applied involute profiles for both drive and coast flanks of the buttress or, as he called them, "hook-tooth" gears. He suggested the 15° pressure angle for drive flanks and the 35° pressure angle for coast flanks.

Many gear researchers [4–11] have defined asymmetric gear geometry traditionally by the pre-selected asymmetric generating gear rack parameters, which are typically modified from the standard symmetric rack by increasing the pressure angle of one flank. The opposite flank and other rack tooth proportions remain unchanged.

It is well known that gear transmission load capacity and power density depend mainly upon the tooth flank surface durability, which is defined by the contact stress level and scuffing resistance. From this point, the application of a higher pressure angle for drive tooth flanks and a lower pressure angle for coast tooth flanks is more promising than the buttress tooth shape. In addition, this tooth form provides lower stiffness and better gear mesh impact dampening.

Prof. E.B. Vulgakov had applied his theory of generalized parameters to asymmetric gears [12, 13], defining their geometry without using rack generation parameters.

Publications [14–17] suggested an asymmetric tooth formed with two involutes of two different base circles. Figure 2 shows that the symmetric tooth with identical drive pressure angle and tooth thicknesses at the reference and tip diameters has a much shorter involute active involute flank than the drive flank of an asymmetric tooth.

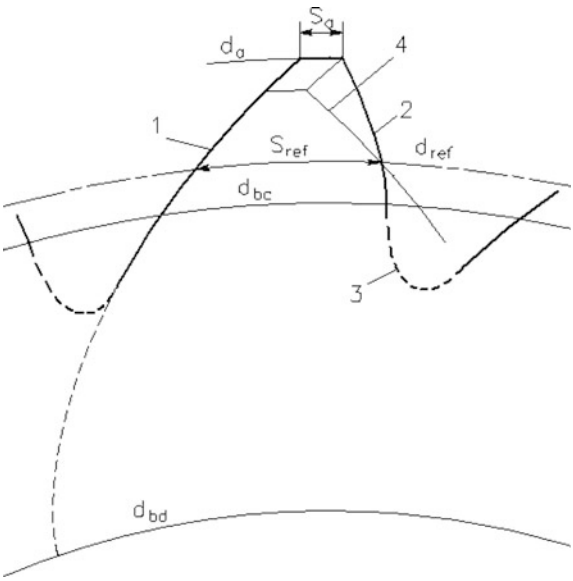

Fig. 2 Asymmetric tooth constructed with two involutes; *1* drive flank from base diameter d_{bd}, *2* coast flank from base diameter d_{bc}, *3* root fillet, *4* symmetric tooth profile with the same drive flank, and tooth thicknesses S_{ref} and S_a at the reference diameter d_{ref} and the tooth tip diameter d_a

The Direct Gear Design approach [18], based on Prof. E.B. Vulgakov's theory of generalized parameters, allowed for maximizing the performance of asymmetric tooth gears. Asymmetric tooth profiles make it possible simultaneously to increase the contact ratio and operating pressure angle beyond those limits achievable with conventional symmetric gears. The main advantage of asymmetric gears is contact stress reduction on the drive flanks that results in higher power transmission density (load capacity per-gear size). Another important advantage is the possibility of designing the coast tooth flanks independently from the drive tooth flanks, i.e., managing tooth stiffness while keeping a desirable pressure angle and contact ratio of drive flanks. This allows for an increase in tooth tip deflection, thus damping tooth mesh impact and resulting in a reduction of gear noise and vibration.

2 Geometry of Asymmetric Tooth Gears

Two involute flanks of the asymmetric tooth (see Fig. 3) are unwound from two different base diameters d_{bd} and d_{bc}. The symbol "*d*" is used for the drive flank and the symbol "*c*" is used for the coast flank of an asymmetric tooth. A diameter dx at the drive flank point *X* can be defined from (1)

$$d_x = d_{bd}/\cos\alpha_{xd} = d_{bc}/\cos\alpha_{xc}. \tag{1}$$

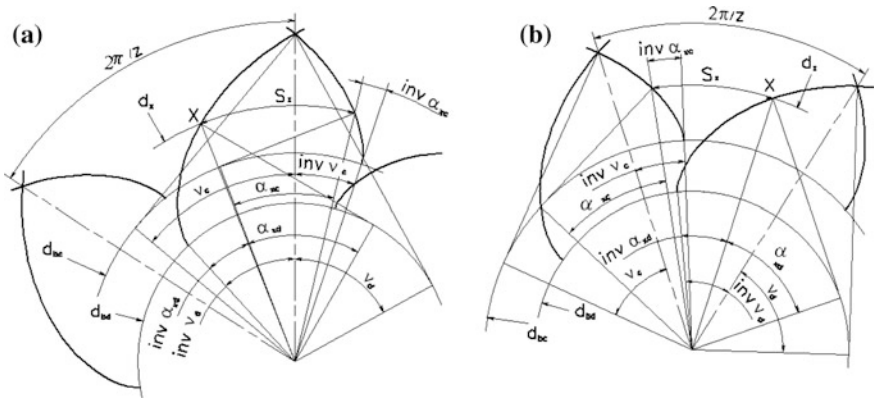

Fig. 3 Involute flanks of external (**a**) and internal (**b**) asymmetric gear teeth, z number of teeth

Then, the tooth asymmetry factor K is

$$K = d_{bc}/d_{bd} = \cos \alpha_{xc}/\cos \alpha_{xd}. \tag{2}$$

For many applications, the drive flank profile angle α_{xd} is greater than the coast flank profile angle α_{xc}. This means $d_{bd} < d_{bc}$ and the asymmetry factor $K > 1.0$.

At the coast flank base circle d_{bc}, the coast flank profile angle $\alpha_{xc} = 0$ and the drive flank profile angle α_{xd} from (2) is

$$\alpha_{xd} = \arccos\left(1/K\right). \tag{3}$$

The base tooth thickness of the asymmetric tooth can be defined only at the coast flank base circle d_{bc}:

- for external tooth

$$S_b = \frac{d_{bc}}{2} \times (inv(v_d) + inv(v_c) - inv(\arccos(1/K)), \tag{4}$$

- for internal tooth

$$S_b = \frac{d_{bc}}{2} \times (2\pi/z - inv(v_d) - inv(v_c) + inv(\arccos(1/K)). \tag{5}$$

The tooth thickness at the diameter d_x is

- for external tooth

$$S_x = \frac{d_x}{2} \times (inv(v_d) + inv(v_c) - inv(\alpha_{xd}) - inv(\alpha_{xc})) \tag{6}$$

or

$$S_x = \frac{d_{bd}}{2\cos\alpha_{xd}} \times (inv(v_d) + inv(v_c) - inv(\alpha_{xd}) - inv(\alpha_{xc})); \tag{7}$$

- for internal tooth

$$S_x = \frac{d_x}{2} \times (\frac{2\pi}{z} - inv(v_d) - inv(v_c) + inv(\alpha_{xd}) + inv(\alpha_{xc})) \tag{8}$$

or

$$S_x = \frac{d_{bd}}{2\cos\alpha_{xd}} \times (\frac{2\pi}{z} - inv(v_d) - inv(v_c) + inv(\alpha_{xd}) + inv(\alpha_{xc})). \tag{9}$$

An asymmetric tooth profile also includes the tip land and the root fillet between teeth (see Figs. 4 and 5). The tooth tip diameter d_a can be defined from (1)

$$d_a = d_{bd}/\cos\ \alpha_{ad} = d_{bc}/\cos\ \alpha_{ac}, \tag{10}$$

where α_{ad} and α_{ac} are the drive and coast profile angles at the diameter d_a.

The tooth tip land S_a of the external gear tooth is defined considering tooth tip radii equal to zero from Eq. (6) or (8)

- for external tooth (Fig. 4)

$$S_a = \frac{d_a}{2} \times (inv(v_d) + inv(v_c) - inv(\alpha_{ad}) - inv(\alpha_{ac})) \tag{11}$$

or

$$S_a = \frac{d_{bd}}{2\cos\alpha_{ad}} \times (inv(v_d) + inv(v_c) - inv(\alpha_{ad}) - inv(\alpha_{ac})); \tag{12}$$

- for internal tooth (Fig. 5)

$$S_a = \frac{d_a}{2} \times (2\pi/z - inv(v_d) - inv(v_c) + inv(\alpha_{ad}) + inv(\alpha_{ac})) \tag{13}$$

or

$$S_a = \frac{d_{bd}}{2\cos\alpha_{ad}} \times (2\pi/z - inv(v_d) - inv(v_c) + inv(\alpha_{ad}) + inv(\alpha_{ac})). \tag{14}$$

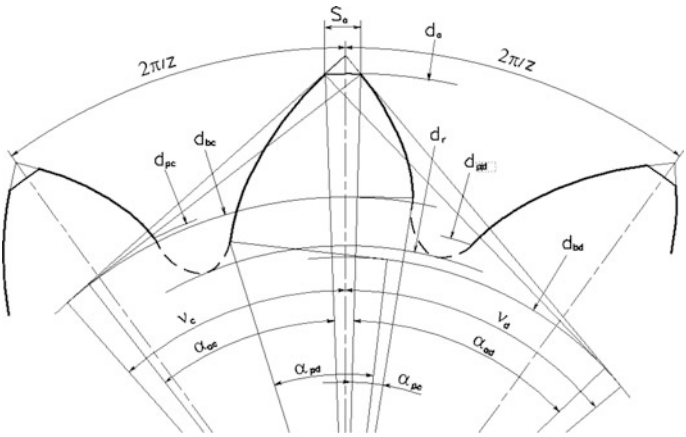

Fig. 4 External asymmetric gear tooth

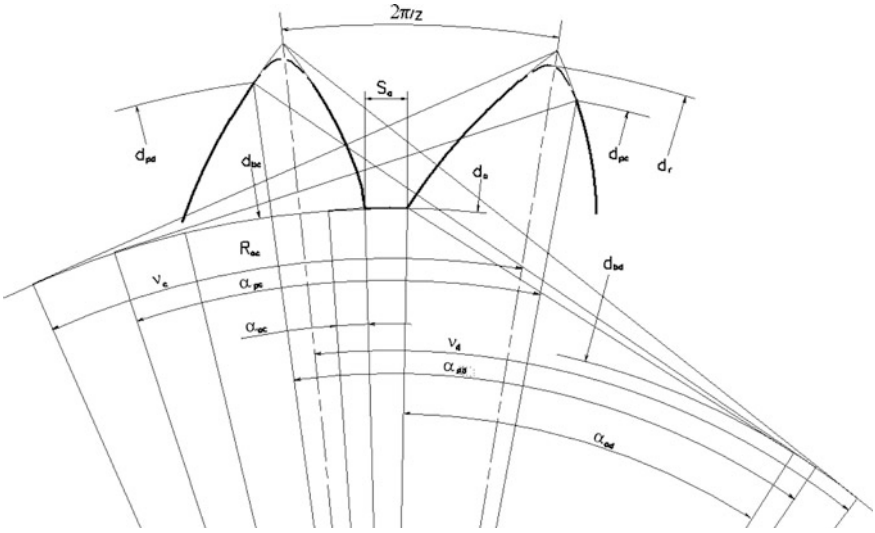

Fig. 5 Internal asymmetric gear tooth

The diameter d_{pd} and d_{pc}, at the last points of contact near the root fillet and related profile angles α_{pd} and α_{pc} are defined considering a mesh with the mating gear. The root diameter d_r is defined as a result of the root fillet profile optimization.

3 Gear Mesh Characteristics

Asymmetric external and internal gear meshes are shown in Fig. 6.

In all figures and equations describing gears with asymmetric teeth, indexes "d" and "c" are for parameters related to the drive and coast tooth flanks accordingly.

The pinion and gear tooth thicknesses S_{w1} and S_{w2} at the operating pitch diameters $d_{w1,2}$ are defined by Eqs. (7) and (9) as

$$S_{w1} = \frac{d_{bd1}}{2\cos\alpha_{wd}}(inv(v_{d1}) + inv(v_{c1}) - inv(\alpha_{wd}) - inv(\alpha_{wc})), \tag{15}$$

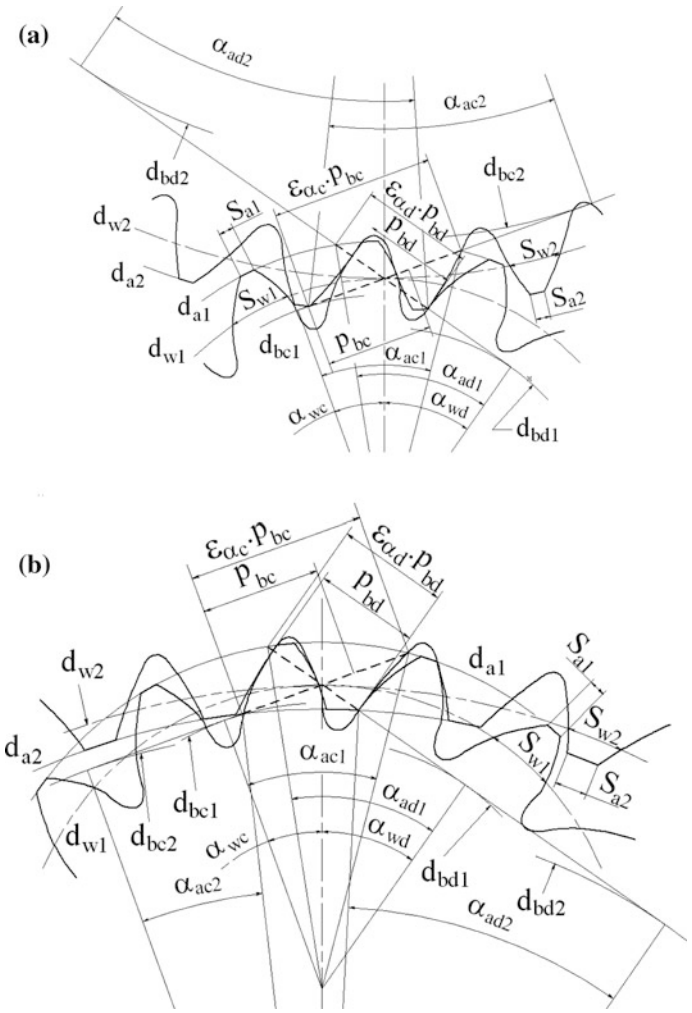

Fig. 6 Asymmetric gear mesh; **a** external, **b** internal

- for external gearing

$$S_{w2} = \frac{d_{bd2}}{2\cos\alpha_{wd}}(inv(v_{d2}) + inv(v_{c2}) - inv(\alpha_{wd}) - inv(\alpha_{wc})), \tag{16}$$

- for internal gearing

$$S_{w2} = \frac{d_{bd2}}{2\cos\alpha_{wd}}(\frac{2\pi}{z_2} - inv(v_{d2}) - inv(v_{c2}) + inv(\alpha_{wd}) + inv(\alpha_{wc})). \tag{17}$$

for the Metric System

$$S_{w2} = \pi m - \frac{d_{bd1}}{2\cos\ \alpha_d}(inv(v_{d1}) + inv(v_{c1}) - inv(\alpha_d) - inv(\alpha_c)), \tag{18}$$

for the English System

$$S_{w2} = \frac{\pi}{DP} - \frac{d_{bd1}}{2\cos\ \alpha_d}(inv(v_{d1}) + inv(v_{c1}) - inv(\alpha_d) - inv(\alpha_c)). \tag{19}$$

The operating pressure angles for the drive flanks α_{wd} and for the coast flanks α_{wc} are defined by substitution of the S_{w1} and S_{w2} from Eqs. (15) and (16) or (17) into the operating circular pitch equation

$$p_w = S_{w1} + S_{w2}. \tag{20}$$

Then, for external gear

$$inv(\alpha_{wd}) + inv(\alpha_{wc}) = \frac{1}{1+u}(inv(v_{d1}) + inv(v_{c1}) + u(inv(v_{d2}) + inv(v_{c2})) - \frac{2\pi}{z_1}), \tag{21}$$

- for internal gear

$$inv(\alpha_{wd}) + inv(\alpha_{wc}) = \frac{1}{u-1}(u(inv(v_{d2}) + inv(v_{c2})) - inv(v_{d1}) + inv(v_{c1})). \tag{22}$$

The relation between pressure angles for the drive flanks α_{wd} and for the coast flanks α_{wc} is defined from (2) as

$$\cos \alpha_{wc} = K \cos \alpha_{wd}. \tag{23}$$

The profile angles at the last points of contact near the fillet are

- for external gear mesh, drive flanks

$$\alpha_{pd1} = \arctan((1+u)\tan \alpha_{wd} - u \tan \alpha_{ad2}), \tag{24}$$

$$\alpha_{pd2} = \arctan(\frac{1+u}{u}\tan \alpha_{wd} - \frac{1}{u}\tan \alpha_{ad1}), \tag{25}$$

- for external gear mesh, coast flanks

$$\alpha_{pc1} = \arctan((1+u)\tan \alpha_{wc} - u \tan \alpha_{ac2}), \tag{26}$$

$$\alpha_{pc2} = \arctan(\frac{1+u}{u}\tan \alpha_{wc} - \frac{1}{u}\tan \alpha_{ac1}), \tag{27}$$

- for internal gear mesh, drive flanks

$$\alpha_{pd1} = \arctan(u \tan \alpha_{ad2} - (u-1)\tan \alpha_{wd}), \tag{28}$$

$$\alpha_{pd2} = \arctan(\frac{u-1}{u}\tan \alpha_{wd} + \frac{1}{u}\tan \alpha_{ad1}), \tag{29}$$

- for internal gear mesh, coast flanks

$$\alpha_{pc1} = \arctan(u \tan \alpha_{ac2} - (u-1)\tan \alpha_{wc}), \tag{30}$$

$$\alpha_{pc2} = \arctan(\frac{u-1}{u}\tan \alpha_{wc} + \frac{1}{u}\tan \alpha_{ac1}). \tag{31}$$

If asymmetry factor $K > 0$, interference occurs first for the coast involute flanks, which are unwound from the larger base circle. If the profile angles α_{pc1} or α_{pc2} in the external mesh or angle α_{pc1} in the internal mesh are less than zero, then their involute flanks close to the base diameters are interfering with the mating tooth tips. This leads to the involute flank profile undercut.

The transverse contact ratios:

- for external gear mesh, drive flanks

$$\varepsilon_{\alpha d} = \frac{z_1}{2\pi}(\tan\alpha_{ad1} + u\tan\alpha_{ad2} - (1+u)\tan\alpha_{wd}), \tag{32}$$

- for external gear mesh, coast flanks

$$\varepsilon_{\alpha c} = \frac{z_1}{2\pi}(\tan\alpha_{ac1} + u\tan\alpha_{ac2} - (1+u)\tan\alpha_{wc}), \tag{33}$$

- for internal gear mesh, drive flanks

$$\varepsilon_{\alpha d} = \frac{z_1}{2\pi}(\tan\alpha_{ad1} - u\tan\alpha_{ad2} + (u-1)\tan\alpha_{wd}), \tag{34}$$

- for internal gear mesh, coast flanks

$$\varepsilon_{\alpha c} = \frac{z_1}{2\pi}(\tan\alpha_{ac1} - u\tan\alpha_{ac2} + (u-1)\tan\alpha_{wc}). \tag{35}$$

4 Asymmetric Tooth Gearing Limits

Figure 7 presents ranges of the drive pressure angles for a different number of teeth and asymmetry factors *K*.

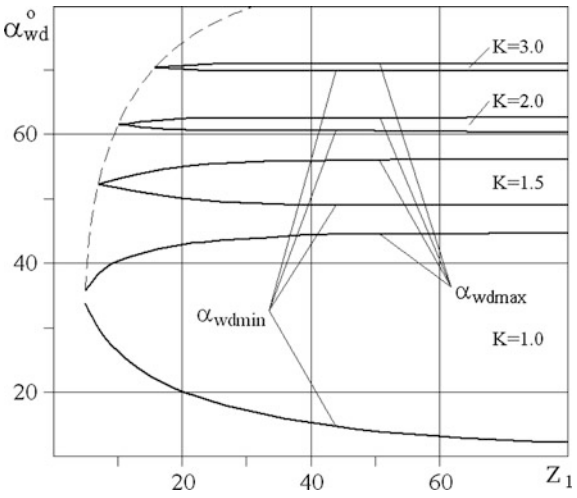

Fig. 7 Minimum and maximum pressure angles for external spur gears with gear ratio $u = 1$ and various asymmetry factors *K*

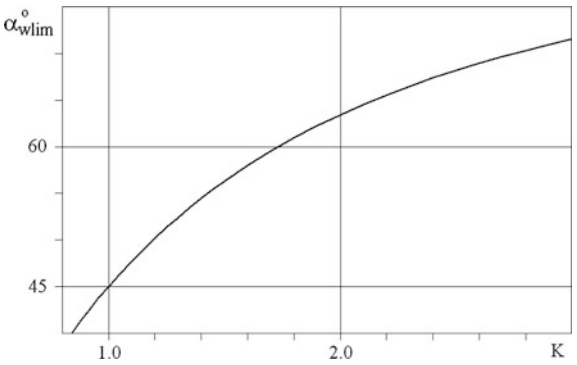

Fig. 8 Pressure angle limits external spur gears

The pressure angle limit for the external spur gears with $z_1 + z_2 \rightarrow \infty$ is [14]

$$\alpha_{\text{wlim}} = \arctan K. \tag{36}$$

A chart of the pressure angle limit α_{wlim} as a function of the asymmetry factor K is shown in Fig. 8.

Direct Gear Design greatly expands the transverse contact ratio range. Its maximum value depends on type of gearing (external or internal), tooth profile (symmetric or asymmetric), number of teeth, and relative tooth tip thicknesses.

Maximum transverse contact ratios for spur external reversible asymmetric gears with the relative tooth tip thicknesses $m_{a1,2} = 0$ are shown in Table 1.

The Table 1 data indicated that the maximum contact ratio of the reversible asymmetric gears is just slightly greater than it is for the symmetric gears, and asymmetry of such gears is very low.

Practical maximum pressure angle and transverse contact ratio are limited by the minimum tooth tip thickness. For a case of hardened teeth, it should be sufficient to avoid the hardening through the tooth tip. For gears made out of soft metals and plastics, it should be sufficient to exclude tooth tip bending. Minimum relative tooth

Table 1 Maximum drive contact ratios for reversible asymmetric gears

Number of teeth, $z_{1,2}$	10	15	20	30	40	50
Drive contact ratio, $\varepsilon_{\alpha d}$	1.53	1.931	2.288	2.924	3.49	4.015
Coast contact ratio, $\varepsilon_{\alpha c}$	1.0	1.0	1.0	1.0	1.0	1.0
Drive flank pressure angle, α°_{wd}	25.67	22.02	19.77	17.02	15.34	14.157
Coast flank pressure angle, α°_{wc}	20.58	15.79	13.19	10.47	8.73	7.692
Drive flank tooth tip angle, $\alpha^{\circ}_{ad1,2}$	43.87	38.97	35.71	31.48	28.75	26.77
Coast flank tooth tip angle, $\alpha^{\circ}_{ac1,2}$	41.51	36.19	32.85	28.71	26.03	24.147
Drive flank lowest involute angle, $\alpha^{\circ}_{pd1,2}$	0.0	0.0	0.0	0.0	0.0	0.0
Asymmetry factor, K	1.039	1.038	1.035	1.028	1.025	1.022

tip thickness typically is $m_{a1,2} = 0.25-0.3$. Practical minimal contact ratio for conventional spur gears is about $\varepsilon_{\alpha min} = 1.1-11.15$. For the high contact ratio (HCR) gears, it is about $\varepsilon_{\alpha min} = 2.05-2.1$. These minimal contact ratio values are chosen to avoid its reduction below 1.0 for conventional spur gears and below 2.0 for the HCR spur gears, because of manufacturing and assembly tolerances, and tooth tip chamfers or radii. These conditions also identify the practical maximum pressure angle. The practical minimal pressure angle for symmetric gears is defined by the beginning of the tooth involute undercut, when the involute profile angles at the lowest contact points $\alpha_{pd1,2} = 0°$, and where the transverse contact ratio reaches its maximum value $\varepsilon_{\alpha max}$.

Practical maximum drive flank pressure angles for conventional and HCR asymmetric gears are shown in Tables 2 and 3 [18].

The maximum drive pressure angle values in Tables 2 and 3 assume some possible small undercut of the coast flank near the root, especially for gears with a low number of teeth (15–30). However, this does not reduce the coast flank contact below $\varepsilon_{\alpha c} = 1.0$.

Table 2 Practical α_{wdmax} for conventional asymmetric gears $(m_{a1,2} = 0.3, \varepsilon_{\alpha d} = 1.1, \alpha_{wc} = 15°)$

z_2	z_1						
	15	20	30	40	50	70	100
15	43.5						
20	44.5	45.5					
30	45.9	46.4	47.3				
40	47	47.3	47.7	48.2			
50	47.6	47.8	48	48.3	48.9		
70	48	48.2	48.6	48.7	49	49.5	
100	48.7	48.9	49.2	49.5	49.1	49.6	50

Table 3 Practical α_{wdmax} for HCR asymmetric gears $(m_{a1,2} = 0.3, \varepsilon_{\alpha d} = 2.1, \alpha_{wc} = 15°)$

z_2	z_1						
	20	25	30	40	50	70	100
20	19.3						
25	20.5	21.5					
30	21.5	22.4	23				
40	23	23.6	24.1	25			
50	24.1	24.6	25	25.6	26.1		
70	25.5	25.8	26.1	26.6	26.9	27.5	
100	26.7	27	27.2	27.5	27.7	28.1	28.5

5 Tooth Geometry Optimization

5.1 Asymmetry Factor K Selection for Reversible Asymmetric Tooth Gears

There are many gear drives where a gear pair transmits the load in both load directions, but with significantly different magnitude and duration (Fig. 9). In this case, the asymmetry factor K for a gear pair is defined by equalizing potential accumulated tooth surface damage defined by operating contact stress and number of the tooth flank load cycles. In other words, the contact stress safety factor S_H should be the same for the drive and coast tooth flanks. This condition can be presented as

$$S_H = \frac{\sigma_{HPd}}{\sigma_{Hd}} = \frac{\sigma_{HPc}}{\sigma_{Hc}}, \tag{37}$$

where:

σ_{Hd} and σ_{Hc} operating contact stresses for the drive and coast tooth flanks,
σ_{HPd} and σ_{HPc} permissible contact stresses for the drive and coast tooth flanks that depend on the number of load cycles

Then, from (37)

$$\frac{\sigma_{Hd}}{\sigma_{Hc}} = \frac{\sigma_{HPd}}{\sigma_{HPc}}. \tag{38}$$

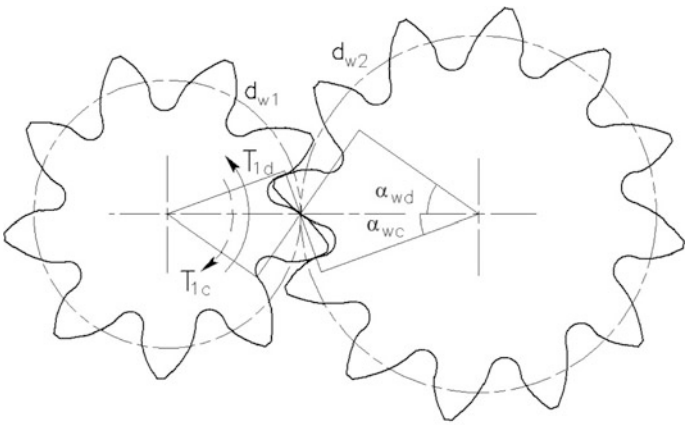

Fig. 9 Asymmetric gear pair; T_{1d} and T_{1c}—pinion torque applied to the drive and coast tooth flanks

The contact stress at the pitch point [19] is

$$\sigma_H = z_H z_E z_\varepsilon z_\beta \sqrt{\frac{F_t}{d_{w1} b_w} \frac{u \pm 1}{u}}, \tag{39}$$

where:

$z_H = \sqrt{\frac{2\cos(\beta_b)\cos(\alpha_{wt})}{\cos(\alpha_t)^2 \sin(\alpha_{wt})}}$ zone factor that, for the directly designed spur gears, is

$$z_H = \frac{2}{\sqrt{\sin(2\alpha_w)}}; \tag{40}$$

Z_E elasticity factor that takes into account gear material properties (modulus of elasticity and Poisson's ratio);
Z_ε contact ratio factor, its conservative value for spur gears is $Z_\varepsilon = 1.0$;
Z_β helix factor, for spur gears $Z_\beta = 1.0$;
F_t nominal tangent load, that, at the pitch diameter d_{w1}, is $F_t = \frac{2T_1}{d_{w1}}$;
T_1 pinion torque;
b_w contact face width;

sign "+" for external gearing, sign "−" for internal gearing.

Then, for the directly designed spur gears, the contact stress at the pitch point can be presented as

$$\sigma_H = z_E \frac{2}{d_{w1}} \sqrt{\frac{2T_1}{b_w \sin(2\alpha_w)} \frac{u \pm 1}{u}}. \tag{41}$$

Some parameters of this equation, Z_E, d_{w1}, b_w, and u, do not depend on the rotation direction and Eq. (38) for the pitch point contact can be presented as

$$\frac{\sin(2\alpha_{wc})}{\sin(2\alpha_{wd})} = A, \tag{42}$$

where a parameter A is

$$A = \frac{T_{1c}}{T_{1d}} \left(\frac{\sigma_{HPd}}{\sigma_{HPc}}\right)^2. \tag{43}$$

According to [19], "The permissible stress at limited service life or the safety factor in the limited life stress range is determined using life factor Z_{NT}". This allows for replacing the permissible contact stresses in Eq. (43) for the life factors

$$A = \frac{T_{1c}}{T_{1d}}\left(\frac{Z_{NTd}}{Z_{NTc}}\right)^2. \tag{44}$$

When the parameter A is defined and the drive pressure angle is selected, the coast pressure angle is calculated by Eq. (43) and the asymmetry coefficient K from the common solution of (42) and (23)

$$K = \frac{\sqrt{1 + \sqrt{1 - A^2(\sin 2\alpha_{wd})^2}}}{\sqrt{2}\cos\alpha_{wd}}. \tag{45}$$

If the gear tooth is equally loaded in both main and reversed load application directions, then both the coefficient A and the asymmetry factor K are equal to 1.0 and the gear teeth are symmetric.

Example #1 The drive pinion torque T_{1d} is two times greater than the coast pinion torque T_{1c}. The drive tooth flank has 10^9 load cycles and the coast tooth flank has 10^6 load cycles during the life of the gear drive. From the S-N curve [19] for steel gears, an approximate ratio of the life factors $Z_{NTd}/Z_{NTc} = 0.85$. Then, the coefficient $A = 0.85^2/2 = 0.36$. Assuming the drive pressure angle is $\alpha_{wd} = 36^o$, the coast pressure angle from Eq. (42) is $\alpha_{wc} = 10^o$ and the asymmetry factor from Eq. (45) is $K = 1.22$.

5.2 Root Fillet Optimization

In Direct Gear Design, the tooth fillet is designed after the involute flank parameters are completely defined. One goal is to achieve a minimum of stress concentration on the tooth fillet profile. In other words, the maximum bending stress should be evenly distributed along the large portion of the root fillet. The initial root fillet profile is a trajectory of the mating gear tooth tip in the tight (zero backlash) mesh. This allows for the exclusion of interference with the mating gear tooth.

The fillet optimization method was developed by Shekhtman [20, 21]. It utilizes the following calculation processes:

- Definition of a set of mathematical functions used to describe the optimized fillet profile. Such a set may contain the trigonometric, polynomial, hyperbolic, exponential, and other functions and their combinations. Parameters of these functions are defined during the optimization process.
- FEA with the triangle linear elements is used to calculate stress. This kind of finite elements make possible the achievement of satisfactory optimization results within a reasonable time.
- A random search method [22] is used to define the next step in the multi-parametric iteration process of the fillet profile optimization.

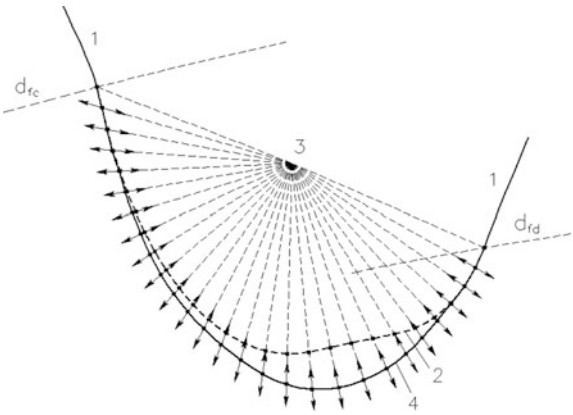

Fig. 10 Tooth fillet profile optimization; *1* involute tooth flanks, *2* initial fillet profile, *3* fillet center, *4* optimized fillet profile, *dfd*, *dfc*—drive and coast flank form circle diameters accordingly

This fillet optimization method establishes the approximate fillet center (Fig. 10). It is defined as the center of the best-fitted circular arc and is connected to the finite element nodes located on the initial fillet profile. The first and last finite element nodes of the initial fillet profile located on the formed diameter circle cannot be moved during the optimization process. The rest of the initial fillet finite element nodes are moved along the straight lines that pass through the fillet center. The bending stresses are calculated for every fillet profile configuration iteration. Variable parameters of the fillet profile functions that describe the fillet profile for the next iteration are defined depending on the stress calculation results of the previous iteration. If it provided stress reduction, the optimization process moves the fillet nodes in the same direction. If stress was increased, the nodes are moved in opposite directions. After the specified number of iterations, the optimization process no longer results in the optimized fillet profile. When more finite element nodes are placed on the fillet profile, stress calculation results are even more accurate, but this requires more iterations, and the fillet profile optimization takes more time. During the optimization process, the fillet nodes cannot be moved inside the initial fillet profile because this may cause interference with the mating gear tooth tip. This is one of the main constraints of fillet optimization.

Figure 11 presents the gear tooth stress distribution comparison before and after root fillet optimization.

Figure 12 presents a comparison of different tooth root fillet profile options. The involute flanks, face widths, tooth load and its application point are the same for all fillet profile options. Results of the FEA stress calculation, along with other root fillet parameters, are shown in Table 4. Calculation results for fillet profile option #1 generated by the standard 20° pressure angle rack profile are considered to be the 100 % benchmark values. Parameters of other fillet profile options are defined relative to option #1.

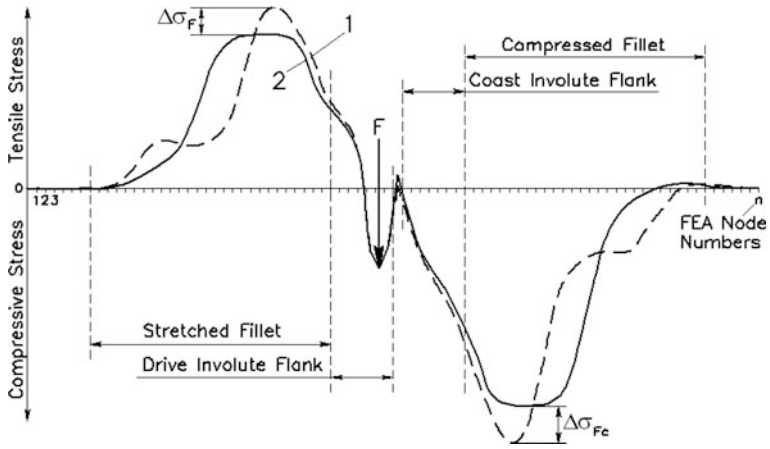

Fig. 11 Tooth profile stress distribution charts before (*1*) and after (*2*) root fillet optimization, $\Delta\sigma_F$ tensile stress reduction, $\Delta\sigma_{Fc}$ compressive stress reduction

The root fillet profile comparison results presented in Table 4 indicate considerable root stress concentration reduction provided by the fillet optimization. At the maximum tensile stress, the point of the optimized fillet has significantly larger fillet radius *Rf*, as well as the smaller distance H and root clearance C. It has the lowest maximum bending stress, which is evenly distributed along the large portion of the fillet profile. Other fillet profiles have significantly greater and more sharply concentrated maximum stress.

Analysis of the fillet optimization results had indicated that the optimized fillet profile practically does not depend on the force value and its application point on the involute flank, except in the case when the application point is located very close to the form diameter. In this case, compression under the applied force may affect the optimized fillet profile. Such load application should not be considered for fillet optimization, because it induces minimal tensile stress in the root fillet in comparison to other load application points along the tooth flank.

The gears with optimized root fillets are shown in Fig. 13.

6 Analytical and Experimental Comparison Symmetric and Asymmetric Tooth Gears

Directly designed gears with an asymmetric involute gear tooth form were analyzed to determine their bending and contact stresses relative to symmetric involute gear tooth form, which is representative of the helicopter main drive gears developed by the Rotorcraft division of the Boeing Company [23]. Asymmetric and baseline (symmetric) toothed gear test specimens were designed, fabricated and tested to

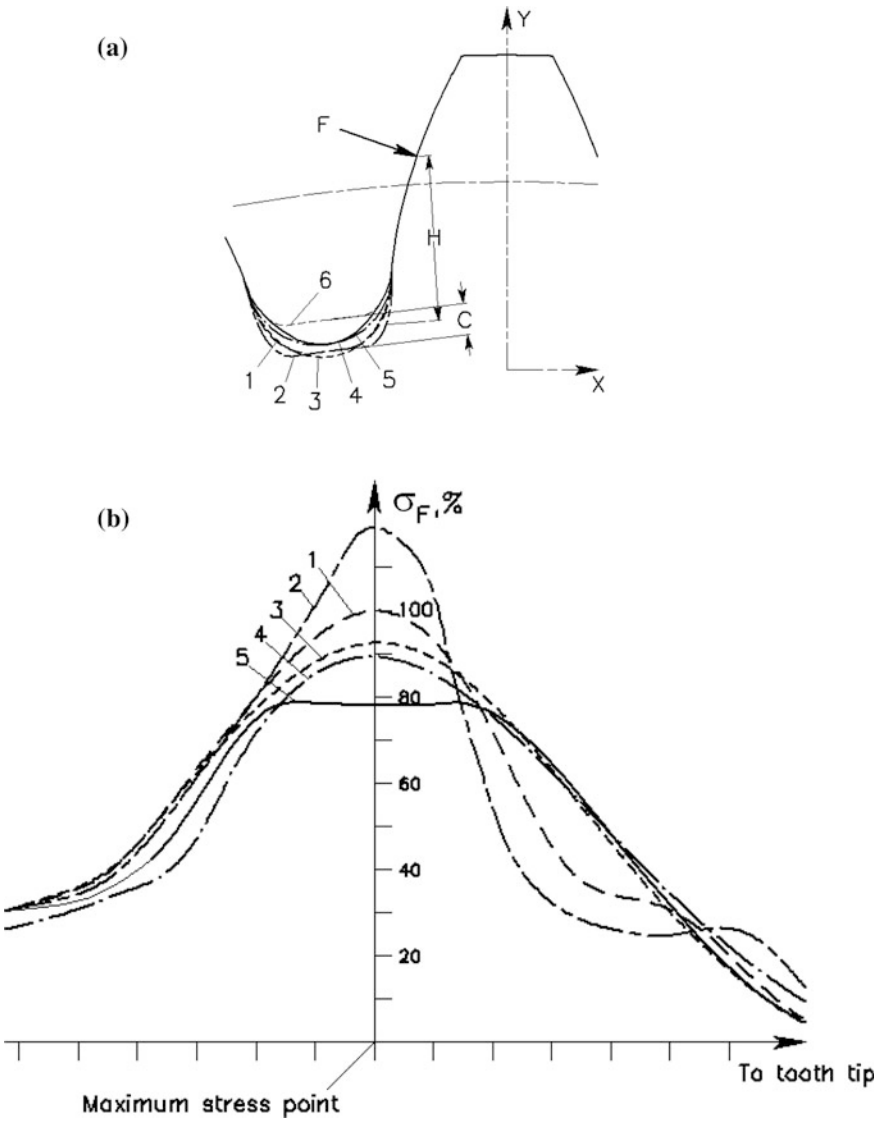

Fig. 12 Root fillet comparison: **a** gear tooth with different fillet profiles; **b** stress chart along the fillet; *1* fillet profile generated by the standard coarse pitch rack with the tip radius 0.3 m; *2* fillet profile generated by the standard fine diametral pitch rack with the tip radius equal to zero; *3* fillet profile generated by the full tip radius rack; *4* circular fillet profile; *5* optimized fillet profile; *6* trajectory of the mating gear tooth tip in tight mesh; *F* applied load; *H* radial distance between load application and max. stress points; *C* radial clearance; R_f fillet curvature radius at the max. stress point; σ_F tensile stress

Table 4 Fillet profile comparison (Fig. 12)

	Rack with tip radius R = 0.3 m	Rack with tip radius R = 0	Rack with full tip radius	Circular fillet profile	Optimized fillet
Fillet profile #	1	2	3	4	5
R_f (%)	100	58	118	121	273
H (%)	100	103	100	88	82
C (%)	100	100	118	79	76
σ_{Fmax} (%)	100	119	90	88	78

Fig. 13 Gears with optimized root fillets

experimentally determine their single-tooth bending fatigue strength and scuffing resistance. The gear test specimens are presented in Fig. 14.

The gear parameters and FEA-calculated bending stresses for the single tooth bending fatigue (STBF) test gears are presented in Table 5.

Similarly, the scuffing test gears are within the design experience range of typical main transmission helicopter power gears. The gear parameters for the scuffing test gear specimens are presented in Table 6.

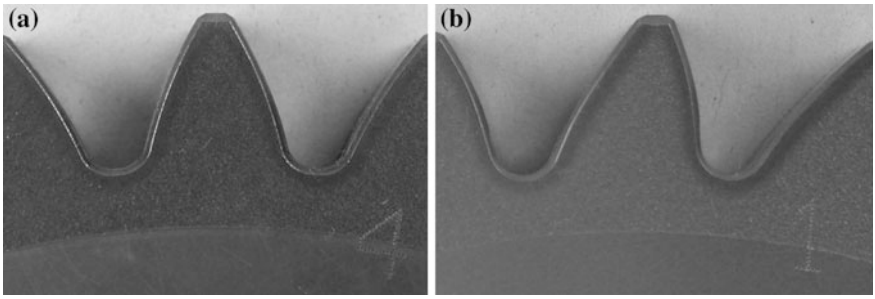

Fig. 14 Test specimen gear tooth profiles; **a** baseline gear teeth, **b** symmetric gear teeth with optimized fillet, **c** asymmetric gear teeth. (Courtesy of Boeing Co, Philadelphia, PA)

Table 5 STBF test gear specimen parameters

	Symmetric gears with circular fillets (baseline)	Asymmetric gears with circular fillets
Number of teeth of both mating gears	32	32
Diametral pitch (1/in)	5.333	5.333
Pressure angle	25°	35°/15°[a]
Pitch diameter (in)	6.000	6.000
Base diameter (in)	5.4378	4.9149/5.7956[a]
Outside diameter (in)	6.3975	6.3864
Root diameter (in)	5.571	5.558
Form diameter (in)	5.6939	5.6581/5.8110[a]
Circular tooth thickness (in)	0.2895	0.2895
Face width (in)	0.375	0.375
Torque (in–lb)	5000	5000
Load application radius (in)	3.06	3.06
Calculated maximum Bending stress (psi)	57,887	54,703 (−5.5 %)

[a]Drive/coast flank parameter

Fatigue results of the single tooth bending fatigue tests of the asymmetric tooth and the baseline specimens are presented in Fig. 15.

Figure 16 shows the scuffing results for baseline and asymmetric gears. The 35° pressure angle asymmetric gears showed an improvement of approximately 25 % in mean scuffing load (torque) compared to the baseline symmetric tooth specimens. The Mean—3 Sigma levels are also shown, based on a population of 8 baseline data points and 6 asymmetric data points.

Test results demonstrated higher bending fatigue strength for both asymmetric tooth forms compared to baseline designs. Scuffing resistance was significantly increased for the asymmetric tooth form compared to a traditional symmetric involute tooth design.

Table 6 Scuffing test gear specimen parameters

	Symmetric gears with circular fillets (baseline)	Asymmetric gears with circular fillets
Number of teeth of both mating gears	30	30
Diametral pitch (1/in)	5.000	5.000
Pressure angle	25°	35°/18°
Pitch diameter (in)	6.000	6.000
Base diameter (in)	5.4378	4.9149/5.7063[a]
Outside diameter (in)	6.400 max	6.403 max
Root diameter (in)	5.459 max	5.510
Form diameter (in)	5.6864	5.6415/5.7607[a]
Circular tooth Thickness (in)	0.3096	0.3096
Face width (in)	0.50	0.50
Drive contact ratio	1.417	1.25
Torque (in-lb)	6000	6000
Calculated maximum Contact stress (psi)	193,180	174,100 (−9.9 %)

[a]Drive/coast flank parameter

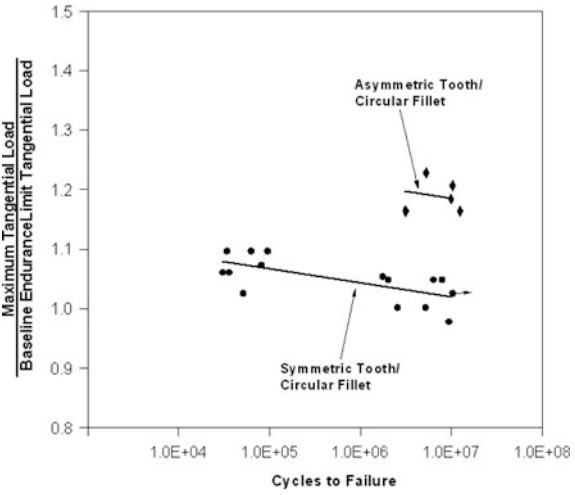

Fig. 15 STBF data for asymmetric gears and optimized root fillet gears along with baseline symmetric tooth/circular fillet test data

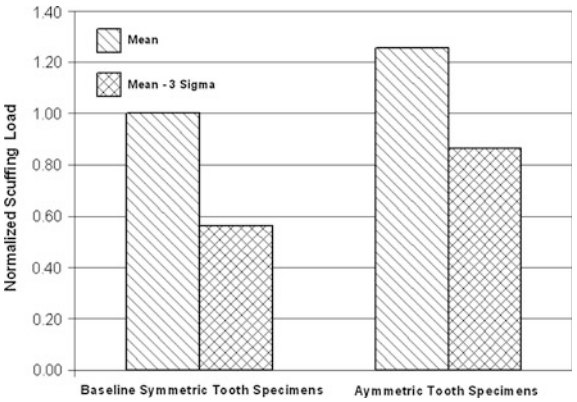

Fig. 16 Results of baseline symmetric and asymmetric gear scuffing tests

7 Implementation of Asymmetric Tooth Gears

The first application of gears with asymmetric teeth in the aerospace industry was for the TV7-117S turboprop engine gearbox [24]. The engine and gearbox were developed by the Klimov Corporation (St. Petersburg, Russia) for a commuter airplane Ilyushin Il-114. The main characteristics of its gearbox are presented in Table 7.

The TV7-117S gearbox arrangement is shown in Fig. 17. The first planetary-differential stage has three planet gears. The second "star" type coaxial stage has five planet (idler) gears and a stationary planet carrier. The first stage sun gear is connected to the engine turbine shaft via spline. Its ring gear is connected with the second stage sun gear and its planet carrier is connected to the second stage ring gear and the output propeller shaft. This arrangement makes it possible to transmit about 33 % of the engine power through the first stage carrier directly to the propeller shaft, bypassing the second stage. This allows for reducing the size and weight of the second stage, because it transmits only 67 % of the engine power

Table 7 TV7–117S turboprop engine data

Input turbine (RPM)	17,500
Output prop (RPM)	1200
Total gear ratio	14.6:1
Overall dimensions (mm):	
• Diameter	520
• Length	645
Gearbox weight (N)	1050
Maximum output power (hp)	2800
Extreme output power (hp)	3500

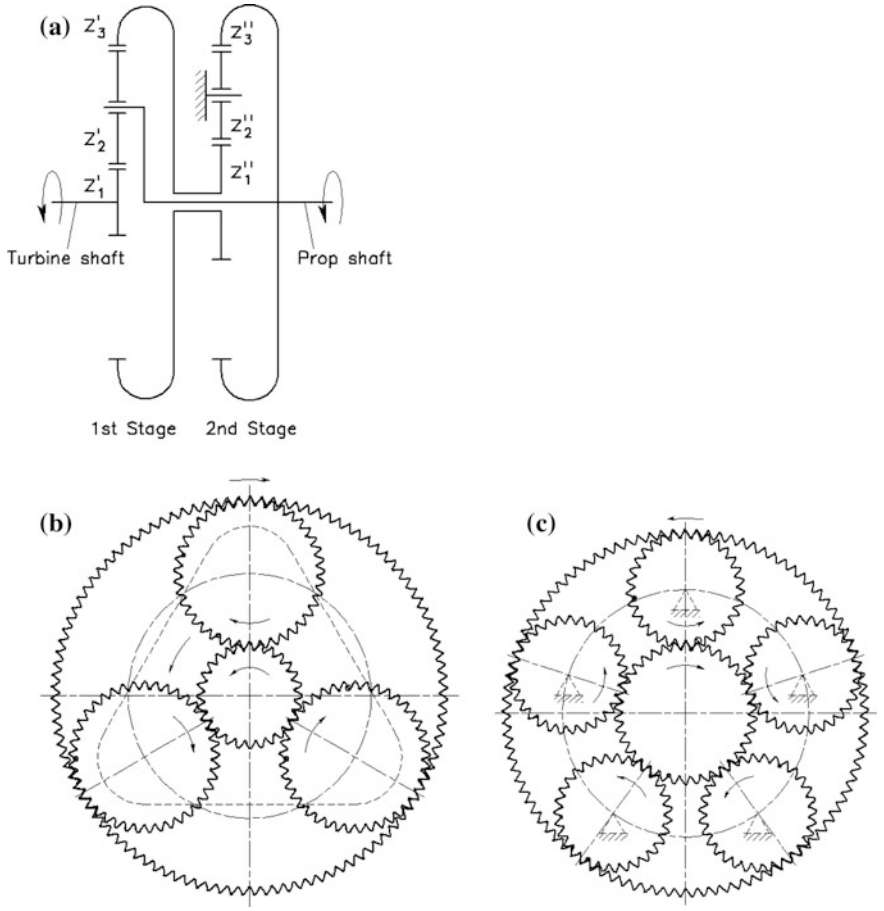

Fig. 17 Gearbox arrangement (**a**), first (**b**) and second (**c**) stages with rotation directions (view from input shaft)

from the first stage ring gear to the second stage sun gear, and then through the planets to the second stage ring attached to the propeller shaft.

All gears have an asymmetric tooth profile. Gear geometry parameters, operating torques and stresses are presented in Table 8.

All gears were made out of the forged blanks of the steel 20KH3MVF (EI-415). Its chemical composition includes: Fe—base material, C—0.15 to 0.20 %, S—<0.025 %, P—<0.030 %, Si—0.17 to 0.37 %, Mn—0.25 to 0.50 %, Cr—2.8 to 3.3 %, Mo—0.35 to 0.55 %, W—0.30 to 0.50 %, Co—0.60 to 0.85 %, Ni—<0.5 %.

Table 8 Gear geometry data

Stage	1st			2nd		
Gear	Sun	Planet	Ring	Sun	Planet	Ring
Number of gears	1	3	1	1	5	1
Nominal number of teeth	28	41	107	38	31	97
Module (mm)	3.000	3.000	3.000	3.362	3.362	3.362
Nominal drive pressure angle (°)	33	33 & 25	25	33	33 & 25	25
Nominal coast pressure angle (°)	25	25 & 33	33	25	25 & 33	33
Nominal pitch diameter (mm)	84.000	123.000	321.000	127.756	104.222	326.114
Drive base diameter (mm)	70.448	103.156 & 111.476	290.925	107.145	87.408 & 94.457	295.56
Coast base diameter (mm)	76.13	111.476 & 103.156	269.213	115.786	94.457 & 87.408	273.502
Tooth tip diameter (mm)	90.02/90.16	128.44/128.6	323.88/324.11	134.07/134.23	110.93/111.07	329.67/329.9
Root diameter (mm)	76.55/77.05	114.55/115.05	337.50/337.7	118.56/119.06	95.45/95.95	345.00/345.2
Tooth thickness at nominal pitch diameter (mm)	4.773/4.814	4.325/4.365	−0.667/ −0.621	4.972/5.018	5.253/5.299	−1.104/ −1.059
Face width (mm)	34.75/ 35	31.75/32	25.48/26	37.75/38	34.75/35.00	27.48/28.00
Center distance (mm)	103.50 ± 0.01			116.00 ± 0.01		
Tolerance analysis results						
Operating drive pressure angle (°)	32.98/33.02		29.87/29.93	32.99/33.03		29.88/29.93
Operating coast pressure angle (°)	24.97/25.03		36.64/36.68	24.98/25.04		36.65/36.68
Operating drive contact ratio	1.18/1.26		1.33/1.36	1.20/1.28		1.35/1.38
Operating coast contact ratio	1.33/1/42		1.18/1.21	1.36/1.44		1.21/1.24
Operating normal backlash (mm)	0.196/0.322		0.197/.406	0.189/0.32		0.206/0.414

(continued)

Table 8 (continued)

Stress analysis results									
Maximum power (hp)		2800							
RPM		17500		−11132		−3063	−3063	3755	1200
Torque per mesh (Nm)		374		548		1430	858	700	2191
Bending Stress (MPa)	Tension	240	257	280	298	289	318	345	371
	Compression	−384	−403	−306	−355	−470	−500	−385	−430
Contact stress (MPa)		960		604		1043		809	

Fig. 18 First and second stage assemblies

Application of the asymmetric teeth helped to provide extremely low weight to output torque ratio, significantly reduced the noise and vibration level, and cut down on the duration and expense of operational development [24].

Photos of the gear assemblies of the TV7-117S gearbox are shown in Fig. 18.

References

1. Woodbury RS (1958) The first epicyclic gear teeth. ISIS 49(4):375–377
2. Willis R (1841) Principles of mechanism. John W. Parker, London
3. Leutwiler OA (1917) Element of machine design. McGraw-Hill Book Company, London
4. Bolotovsky IA, Vasil'eva OF, Kotelnikov VP (1984) Involute gears with asymmetric teeth. Vestnik Mashinostroeniya 4:15–17
5. DiFrancesco G, Marini S (1997) Structural analysis of asymmetrical teeth: reduction of size and weight. Gear Technology, pp 47–51
6. Gang G, Nakanishi T (2001) Enhancement of bending load carrying capacity of gears using an asymmetric involute tooth. In: Paper presented at the JSME international conference on motion and transmissions (MPT2001-Fukuoka), Fukuoka, Japan
7. Karpat F, Cavdar K, Babalik FC (2005) Computer aided analysis of involute spur gears with asymmetric teeth. VDI Berichte 1904(I):145–163
8. Brecher C, Schafer J (2005) Potentials of asymmetric tooth geometries for the optimization of involute cylindrical gears. VDI Berichte 1904(I):705–720
9. Yang SC (2007) Study on an internal gear with asymmetric involute teeth. Mech Mach Theory 42:977–994
10. Pedersen NL (2010) Improving bending stress in spur gears using asymmetric gears and shape optimization. Mech Mach Theory 45:1707–1720
11. Wang S, Liu GR, Zhang GY, Chen L (2011) Design of asymmetric gear and accurate bending stress analysis using the ES-PIM with triangular mesh. Int J Comput Methods 8(4):759–772
12. Vulgakov EB, Vasina LM (1978) Involute gears in generalized parameters. Mashinostroenie, Moscow
13. Vulgakov EB, Rivkin GV (1976) Design of gears with asymmetric tooth profile. Mashinovedenie 5:35–39

14. Kapelevich AL (1984) Research and development of geometry of modernized involute gears. Ph.D. Dissertation, Moscow State Technical University
15. Kapelevich AL (1987) Synthesis of asymmetric involute gearing gears. Mashinovedenie 1:62–67
16. Vulgakov EB, Kapelevich AL (1986) Asymmetric gear transmissions: Possible developments. Vestnik Mashinostroeniya 4:14–16
17. Kapelevich AL (2000) Geometry and design of involute spur gears with asymmetric teeth. Mech Mach Theory 35:117–130
18. Kapelevich AL (2013) Direct gear design. CRC Press
19. Standard ISO 6336 (2006) Calculation of load capacity of spur and helical gears
20. Kapelevich AL, Shekhtman YV (2003) Direct gear design: bending stress minimization. Gear Technology, pp 44–49
21. Kapelevich AL, Shekhtman YV (2009) Tooth fillet profile optimization for gears with symmetric and asymmetric teeth. Gear Technology, pp 73–79
22. Rastrigin LA (ed) (1969) Random search theory and application. Zinatne, Riga
23. Brown FW, Davidson SR, Hanes DB, Weires DJ, Kapelevich AL (2011) Analysis and testing of gears with asymmetric involute tooth form and optimized fillet form for potential application in helicopter main drives. Gear Technology, pp 46–55
24. Novikov AS, Paikin AG, Dorofeyev VL, Ananiev VM, Kapelevich AL (2008) Application of gears with asymmetric teeth in turboprop engine gearbox. Gear Technology, pp 60–65